Dust Measurements in the Coma of Comet 81P/Wild 2 by the Dust Flux Monitor Instrument

Anthony J. Tuzzolino, *et al.*

Science **304**, 1776 (2004);
DOI: 10.1126/science.1098759

Science (print ISSN 0036-8075; online ISSN 1095-9203) is published weekly, except the last week in December, by the American Association for the Advancement of Science, 1200 New York Avenue NW, Washington, DC 20005.

nitrogen species are N-heterocyclic fragment ions similar to the nitrogen species seen in Halley (*11*). However, N is electropositive, and thus those species containing N are favored in the production of positive ions. The presence of complex O-containing species as postulated by (*11*) cannot be confirmed. One spectrum (Fig. 1) shows lines where Cr, Fe, and Ni (m/z = 52, 54, 56, and 58) would be; however, it can also be interpreted as $C_3NH_x^+$ (x = 2, 4, 6, 8) because of other homologous species in this spectrum. Moreover, the presence of Fe without at least some Mg, Si, S, or Ca seems very unlikely. The intensities at $m/z = 24^+$, 25^+, 26^+, 32^+, 34^+, 40^+, 44^+, and 48^+ do not match any reasonably assumed isotopic ratio, so they more likely to be part of the organic fraction. The second set of positive-ion spectra start with Na^+ ($m/z = 23^+$) and contain K^+ ($m/z = 39^+$, 41^+), the two known contaminants of the Ag target. In the spectra from Wild 2, $C_6NH_4^+$ ($m/z = 90^+$) is the most prominent ion, and it forms as a contribution of N-containing alicyclics. With N-free and O-free alicyclic polymers, as tested with polystyrene (*5*), with an impact velocity of 6 km/s, only the tropylium ion $C_7H_7^+$ ($m/z = 91^+$) was detected as a prominent organic line in laboratory spectra as an expected nonradical ion by rearrangement of the 7C ring structure due to Debye-Hückel stability (*12*).

If we started with the methylpyridine rearrangement, the 6C-1N ring ($C_6NH_6^+$) would be unstable, because the localized charge at N will cause H_2^- loss during its formation. This second set of positive ions shows an abundance of heterocyclic, probably annealed, rings as backbones of most of the organic structure. The analysis of the third set of spectra is ongoing. They are similar to the second set but have a higher background because of the decay of excited ions.

There is a difference in the number and flux of impacts seen by the unshielded DFMI [Dust Flux Monitor Instrument (*13*)] as compared to CIDA. However, during the flyby of Wild 2, the ratio of the number of CIDA events to that of DFMI events remained nearly constant. CIDA is sensitive to particles >0.1 pg. The difference in the number of measured impacts between the two instruments may be due to the sensitivity of DFMI (>1 pg), the dust shield geometry, and the position of the instrument on the spacecraft, which is favorable for DFMI. Because several scenarios may explain the difference, this issue needs further investigation.

The CIDA mass spectra at Wild 2 are similar to the spectra obtained from Halley, indicating that the two comets have similar chemistry even though they are of different ages, were sampled in different regions of the solar system, and were sampled during different levels of cometary activity. Our spectra from the flyby of Wild 2 at 1.86 astronomical units (AU) from the Sun suggest that all of the water and most of the carbon monoxide were no longer in the dust particles, because we did not see their characteristic mass lines. At Halley, spectra dominated by C^+ and O^+ (atomic ions at the very high impact speed) were found within 5000 km from the nucleus, coinciding with the distance range needed to explain the extended gas source for CO (*14*). Nitrogen chemistry was predominant, whereas C-, N-, and O-containing moieties, such as amino acids, are unlikely to be present, based on our spectra. Sulfur, commonly attributed to mineral phases of cometary dust, may also be an important component of the organic phases, because we see sulfur ions in one of our spectra of negative ions, and this spectrum is associated with organic phases.

References and Notes

1. J. Kissel *et al.*, *Nature* **321**, 280 (1986).
2. J. Kissel *et al.*, *Nature* **321**, 336 (1986).
3. J. Kissel, F. R. Krueger, *Appl. Phys. A* **42**, 69 (1987).
4. J. Kissel *et al.*, *J. Geophys. Res.* **108,** 8114 (2003).
5. J. Kissel, F. R. Krueger, *Rapid Comm. Mass Spectrom.* **15**, 1713 (2001).
6. J. Kissel, F. R. Krueger, unpublished observations.
7. F. R. Krueger *et al.*, *Rapid Comm. Mass Spectrom.* **18**, 103 (2004).
8. J. M. Greenberg, *Sci. Am.* **250**, 124 (1984).
9. C. Muñoz *et al.*, *Nature* **416**, 403 (2002).
10. H. Schulze, J. Kissel, *Meteoritics* **27**, 286 (1992).
11. J. Kissel, F. R. Krueger, *Nature* **326**, 755 (1987).
12. F. W. McLafferty, *Interpretation of Mass Spectra* (University Science Books, Mill Valley, CA, ed. 3, 1980).
13. A. J. Tuzzolino *et al.*, *J. Geophys. Res.* **108**, 8115 (2003).
14. B. Clark, L. W. Mason, J. Kissel, *Astron. Astrophys.* **187**, 779 (1987).
15. The authors thank NASA for the opportunity to fly the CIDA instrument, which was built by von Hoerner und Sulger GmbH, Schwetzingen, Germany, with funds from DARA (the German Space Agency) and with contributions from Institut d'Astrophysique Spatiale/Centre National d'Etudes Spatiales, France; Finnish Meteorological Institute (Finland); Jet Propulsion Laboratory/NASA (USA); and several Max Planck Institutes in Germany.

6 April 2004; accepted 26 May 2004

REPORT

Dust Measurements in the Coma of Comet 81P/Wild 2 by the Dust Flux Monitor Instrument

Anthony J. Tuzzolino,[1] Thanasis E. Economou,[1]* Ben C. Clark,[2] Peter Tsou,[3] Donald E. Brownlee,[4] Simon F. Green,[5] J. A. M. McDonnell,[5] Neil McBride,[5] Melusine T. S. H. Colwell[5]

We present measurements of the dust particle flux and mass distribution from the Stardust Dust Flux Monitor Instrument (DFMI) throughout the flyby of comet 81P/Wild 2. In the particle mass regime from 10^{-14} to 10^{-7} kilograms, the spacecraft encountered regions of intense swarms of particles, together with bursts of activity corresponding to clouds of particles only a few hundred meters across. This fine-scale structure can be explained by particle fragmentation. We estimate that 2800 ± 500 particles of diameter 15 micrometers or larger impacted the aerogel collectors, the largest being ~6×10^{-7} kilograms, which dominates the total collected mass.

Comets are one of the primary sources of interplanetary dust as sublimating gases from their nuclei release and accelerate particles, ranging in size from submicrometer grains to objects many meters across. Particles are accelerated by gas drag within a few nucleus radii of the surface and reach size- and shape-dependent terminal velocities ranging from the gas emission speed itself, approaching 1 km s^{-1} for submicrometer particles, to values of less than 1 m s^{-1} for the largest particles. Their subsequent trajectories are determined by gravity and solar radiation pressure, which depend on the size, structure, and composition of the grains. Although some of these properties can be constrained by remote observations of comae, in situ detection provides a mechanism to directly determine the masses and distribution of particles within the inner coma.

The Dust Flux Monitor Instrument (DFMI) objectives were to support the primary Stardust goal of sample collection and to provide information about the overall coma conditions through measurement of particle spatial and mass distributions throughout the coma. In addition, interplanetary measurements were planned during the cruise phase of the mission. The impact data provided additional information for interpretation of spacecraft health and any possible instrument anomalies that may have resulted from dust impacts. Here, we present

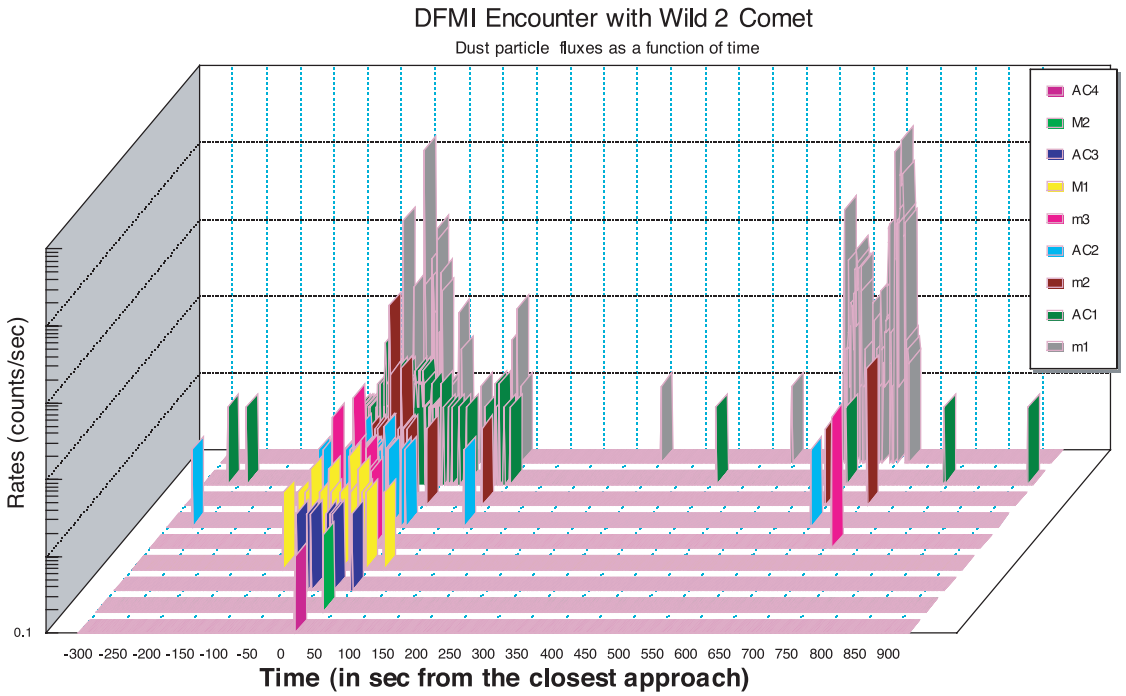

Fig. 1. Counting rates for all of the eight PVDF channels and the four acoustic channels during the Wild 2 encounter. Those channels that have no counts were excluded from the figure. sec, seconds.

initial results from DFMI and discuss the spatial and mass distribution of dust in the coma of 81P/Wild 2.

The DFMI consists of two different dust detector systems: a polyvinylidene fluoride (PVDF) dust sensor unit (SU) (*1*), which measures particles with mass greater than 10^{-14} kg, and a dual acoustic sensor system (DASS), which uses two piezoelectric accelerometers mounted on the first two layers of the spacecraft Whipple dust shield to measure the flux of particles with mass larger than 3×10^{-11} kg.

The PVDF subsystem of the DFMI consists of two separate sensors with different effective areas and sensitivity. The large PVDF sensor has a sensitive area of 200 cm^2 and a thickness of 28 μm. The small PVDF sensor has a sensitive area of 20 cm^2 and a thickness of 6 μm, which is more sensitive to the smaller-sized dust particles. The SU is rigidly mounted to the spacecraft bumper panel and is connected to the DFMI electronics box, which is mounted within the spacecraft body. Each of the two PVDF detector systems has four mass thresholds (m1, m2, m3, and m4 for the small detector and M1, M2, M3, and M4 for the larger detector) (*1*). The values for the mass thresholds are shown in Table 1. Each impacting particle increments a 16-bit threshold counter for the appropriate channel by one, so even if there is a loss of telemetry the total number of impacts is recorded correctly at each DFMI readout. The fast response of the PVDF detectors allows count rates of up to 10^4 s^{-1} to be measured with dead time corrections of less than 5%.

Table 1. Total number of counts measured during the encounter. The second high-activity period occurred after +600 s. Particle diameters are indicative only and are calculated assuming a density of 500 kg m^{-3}.

Channel	Mass threshold (kg)	Particle diameter (μm)	Impacts before +600 s	Impacts after +600 s
m1	9.8×10^{-15}	3	1709	6860
m2	1.2×10^{-13}	8	60	7
m3	4.3×10^{-12}	25	21	5
m4	6.3×10^{-10}	130	0	0
M1	8.5×10^{-11}	70	20	0
M2	1.7×10^{-9}	190	1	0
M3	1.4×10^{-8}	380	0	0
M4	1.5×10^{-7}	830	0	0
AC1 (front)	3×10^{-11}	50	130	3
AC2 (front)	3×10^{-10}	100	40	1
AC3 (rear)	2×10^{-10}	900	7	0
AC4 (rear)	2×10^{-9}	2000	1	0

The limited resources available for the acoustic sensors, and the requirement to measure individual masses for the larger impactors, mean that the transmitted counts do not correspond directly to individual impacts. Instead, an individual impact is characterized by the length of time that the output signal exceeds a voltage threshold. The acoustic detector system has two thresholds for each of its two detectors. The output voltage obtained from the sensors is a complex sinusoidal (frequency ~ 20 kHz) oscillation within an envelope, which has an initial sharp rise to a peak voltage, V_p, and a gradual quasi-exponential decay with a time constant of a few milliseconds. If a single impact occurs between DFMI readouts, then the number of counts is related to the duration of the signal, which can be used to derive V_p and ultimately the mass (*1*). The derivation of a precise mass for an individual impacting particle requires knowledge of the impact position and the detector sensitivity. Because the position is unknown, a given count may be the result of a small impact close to the sensor or a large impact further away. The derived momentum (and therefore mass) of an impactor is therefore represented by a probability function rather than a specific value. This is also true for the mass thresholds corresponding to events that just trigger the sensor. The threshold mass for the front shield acoustic sensor, $m(AC1) = 3 \times 10^{-11}$ kg, is chosen such that about 90% of all detected par-

[1]Laboratory for Astrophysics and Space Research, Enrico Fermi Institute, University of Chicago, 933 East 56th Street, Chicago, IL 60637, USA. [2]Lockheed Martin Astronautics, Post Office Box 179, MS-B0560, Denver, CO 80201, USA. [3]Jet Propulsion Laboratory, California Institute of Technology, Pasadena, CA 91109–8099, USA. [4]Astronomy and Astrophysics Department, University of Washington, Seattle, WA 98195, USA. [5]Planetary and Space Sciences Research Institute, Open University, Walton Hall, Milton Keynes MK7 6AA, UK.

*To whom correspondence should be addressed. E-mail: tecon@tecon.uchicago.edu

ticles have masses larger than this threshold. Although there is some uncertainty in the threshold mass (a conservative value of a factor of 3 is applied here), the upper mass threshold m(AC2) equals 10 m(AC1), defined by the choice of threshold voltages in the instrument. The rear shield sensor detects both remnants of the incident particle and fragments of ejecta from the exit hole of the front shield. The mass threshold corresponding to a detected rear shield signal [which is only marginally larger than the threshold for penetration reported in (*1*)] is $m(\mathrm{AC3}) = (2^{-1.2}/_{+2}) \times 10^{-7}$ kg. The uncertainty has its basis in the scatter in the limited experimental data for different impactor materials. The upper mass threshold, m(AC4), is fixed at precisely 10 times that of m(AC3).

The DFMI on the Stardust spacecraft was activated shortly after launch to monitor interplanetary dust particles. After several months of operation, however, the instrument started to experience thermal problems and would become noisy if left on for long periods. Consequently, the DFMI was left off for most of the remaining cruise period, with occasional activations to test its operation. In each case, it operated nominally for between 35 and 40 min with a well-defined onset of noise (*2*). The decision was therefore taken to operate DFMI for only 30 min, centered on the predicted time of closest approach to Wild 2. The instrument performed nominally at the encounter test [Annefrank asteroid encounter on 2 November 2002 (*3*)] and throughout the Wild 2 encounter itself (*2*).

At Wild 2, the DFMI was activated 15 min before the estimated closest approach time. After activation, it provided quantitative measurements of the dust environment in the coma throughout the entire flyby. Figure 1 gives an overview of the entire data set obtained during the encounter with all detector sensors. The data in Fig. 1 have not been converted to fluxes but are shown as counts to indicate the time sequence of events during the entire flyby. The first dust impact detected by DFMI was with the acoustic sensor at –264 s at a cometocentric distance of $r = 1630$ km (all times and distances are referred to closest approach of 236.4 km at 19:21:32 universal time on 2 January 2004). The event rate gradually increased up to closest approach and then decayed afterward. However, closer inspection of the event rates shows distinct "clumpiness" of the impacts on the detectors. This structure dominates for the smaller particles detected by the PVDF sensors. In addition, almost 80% of the PVDF detections occurred between +620 s ($r = 3810$ km) and +720 s ($r = 4420$ km) after closest approach, but there was only one acoustic event at the larger particle masses in this time interval. The last detected particle was at +922 s at $r = 5650$ km. It is also noticeable that the majority of the acoustic sensor data occurred in the first high-activity period, with very few acoustic sensor impacts seen in the second period. This suggests that the local mass distribution is different during the two high-activity periods. Unexpected high fluxes of low mass ($\geq 10^{-16}$ kg) dust particles at very great distances from the nucleus ($\sim 3 \times 10^5$ to 6×10^6 km) were also reported for comet 1P/Halley (*4*–*6*).

A subset of the data over the time period −50 s to +50 s (within $r = 450$ km) is shown in Fig. 2, which also indicates the correlation between the most sensitive PVDF channel (particle masses from 10^{-14} to 10^{-13} kg) (Fig. 2A) and the most sensitive acoustic sensor channel (particle masses $> 3 \times 10^{-11}$ kg) (Fig. 2B). The data from both sensors have been binned into counts per second. Viewed at this scale, the dust impacts, particularly on the PVDF sensor, are very clumped. There appear to be swarms of events lasting a few seconds (e.g., distinct swarms can be identified between −32 to −26 s, between +2 to +5 s, and between +10 to +17 s) with no events in the intervening period. This unexpected type of activity has not been observed to such a degree in any other cometary encounters. Instruments on the Vega 1 and Vega 2 missions to comet 1P/Halley, each carrying one PVDF sensor (*4*), did identify some enhancements in impact rates, but these were superimposed on a background dust coma (*6*–*9*).

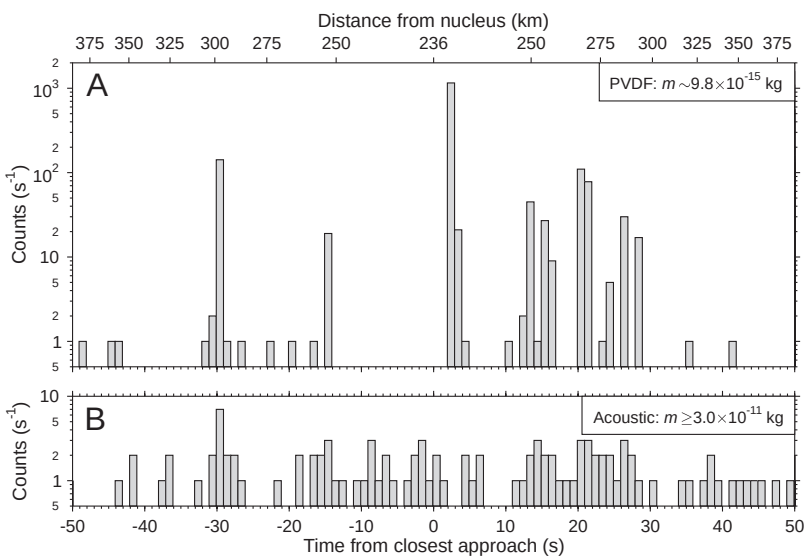

Fig. 2. A subset of the data for (**A**) the most sensitive channels of the PVDF small sensor channels, m1, and (**B**) the acoustic sensor channel AC1. The data are binned into 1-s intervals.

Some swarm events are correlated between the PVDF and acoustic sensors. For example, the −32 s to −26 s swarm appears on both sensors. However, this is not always the case. The most obvious example is the PVDF sensor swarm at +2 s to +5 s. In this event, the PVDF sensor detects over 1100 impacts in about 2 s, whereas the acoustic sensor detects no impacts in the same period.

The data in Fig. 2 was binned into 1-s intervals for comparison between sensors. However, the DFMI readout is designed to assign a resolution of 1 s or 0.1 s. If no events are detected in any of the PVDF sensor channels, the readout occurs at 1-s intervals. However, if an event is detected in any of the PVDF sensor channels, the data are read out 0.1 s later. Therefore, we reconstructed the PVDF data stream at a resolution of 0.1 s throughout the encounter, allowing a closer inspection of the finer-scale structure within apparent swarms of impacts. Although the acoustic data are read out at the same time, it is not possible to obtain a time resolution this high when no PVDF events are detected. We will focus our discussion on an 18-s interval immediately after closest approach (Fig. 3A) (i.e., including the +2 s to +5 s swarm discussed above) and an 18-s interval from the second high-activity period centered at +706 s (Fig. 3B). The swarms consist of short bursts of impacts, a fraction of a second in duration. Some bursts are seen as single events of duration of less than or equal to 0.1 s, surrounded by a relatively silent period lasting up to several seconds.

Structure on such a short time scale (i.e., small physical scale in the coma) was unexpected and offers insight into the physical mechanisms at work in the coma. "Jets" have often been attributed to the emission of dust from discrete active regions on the nucleus, with dust traveling radially away from the local surface normal. However, three-dimensional fluidodynamical coma models [e.g., (*10*)] demonstrate that jets are shocks resulting from nonradial gas flow and depend critically on the nucleus shape and topography (but do not require discrete active regions). This implies that the dust particles in the inner coma are also concentrated along the gas flow discontinuities, creating the visual impression of jets (*11*) even though the dust may originate from different areas on the nucleus surface. Whatever the mechanism for produc-

tion, such features are manifestly visible in near-nucleus images from all cometary flybys to date (*12*–*15*). Because the first high-activity period in the DFMI data contained multiple swarms (Fig. 2), we ask whether these swarms bear any relation to jets visible in the inner coma. At distances from the nucleus where gas drag no longer dominates the forces on a dust grain (dependent on gas production rate and particle size and shape, but above a few tens of nuclear radii), the resultant dust particle trajectories are determined by the terminal velocity when they decouple from the gas flow, gravity, and solar radiation pressure. On global coma scales of tens of thousands of km, radiation pressure dictates the overall coma shape but has little effect within a few hundred km from the nucleus, as sampled by the Stardust near-close approach. The jets visible in the inner coma will merge into a background coma as the cometocentric distance increases. If we assume the extreme case that particles in a jet have terminal velocities that extend in a direction radially outward from the nucleus, the angular width of the observed jets can be compared with the structures seen in DFMI data. Nonradial trajectories would result in broader features that rapidly merge into a uniform coma. The swarms (Fig. 2) that occur between −32 s to −28 s, +2 to +5 s, and +12 s to +17 s correspond to angular sizes (assuming Stardust passes through the center of the jets) of between about 4° and 7°, which are consistent with the typical angular widths of optical jets seen in the images (*12*, *13*). However, there are no apparent structures in the images with angular sizes ~ 0.1°, which are implied by the burst durations. The second high-activity period has a duration of ~100 s and occurs when Stardust is between 3800 km and 4400 km from the nucleus, just after crossing of the terminator plane. The angular size is only 0.5°, and the individual swarms within this period have an angular size of only ~0.01°.

Several characteristics of the coma structure highlighted above differ from previous observations and inferences from coma models, namely the small physical size (short duration) of the bursts, the relative intensity of the swarms and bursts compared with the background flux, and the sharp transitions between regions of high and low (or zero) impacts. All can be explained by grain fragmentation. The very high level, but short duration, bursts are the result of the spacecraft passing through a compact cloud of fragmentation products. A swarm (i.e., a jet crossing) may contain one or more (or no) bursts, resulting in a wide variety of local size distributions. The correlation, or lack of correlation between the small (PVDF) and larger (acoustic) events shown in Fig. 2 may give some additional insight to when the fragmentation occurs. If fragmentation occurs well outside the gas acceleration zone, then the large and small particles will continue to travel together away from the nucleus. Thus, a swarm of impacts would be seen on both PVDF and acoustic sensors. However, if fragmentation occurs within the acceleration zone, then the smaller particles will be physically displaced from the larger particles, resulting in detection of only a narrow range of sizes by the

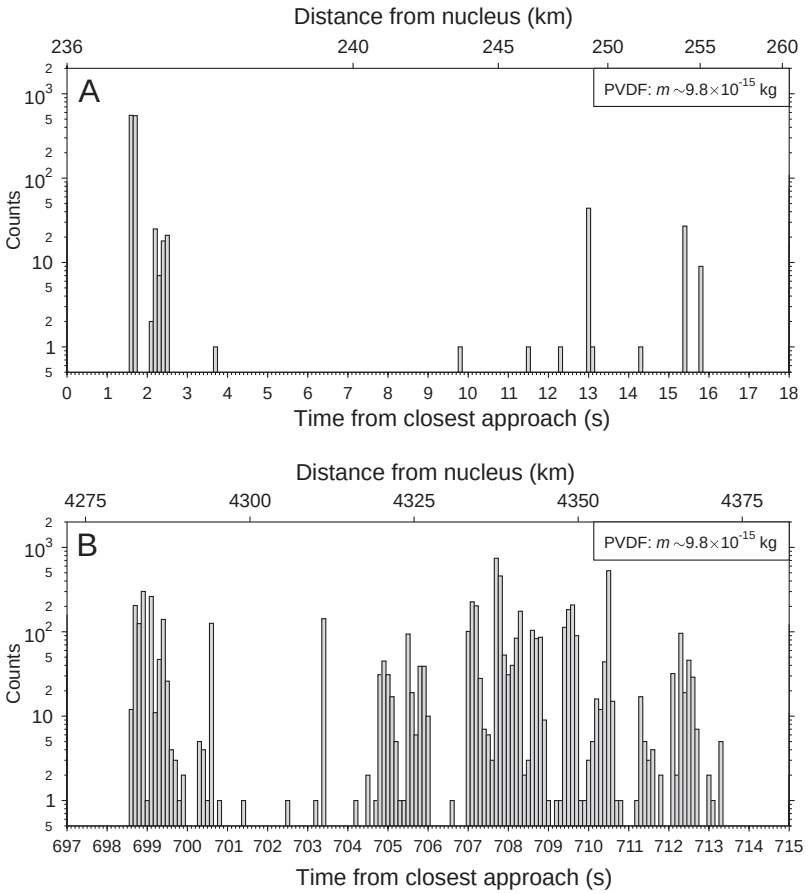

Fig. 3. A subset of the data for the most sensitive channel of the PVDF small sensor (m1). The data are shown at the highest resolution of 0.1-s intervals. (**A**) 18 s immediately after closest approach. The swarm occurring between about 1 and 4 s, which in Fig. 2 appears continuous, is actually a series of bursts of duration < 0.1 s. (**B**) 18 s of data when the spacecraft is about 4300 km from the nucleus (during the second high-activity period).

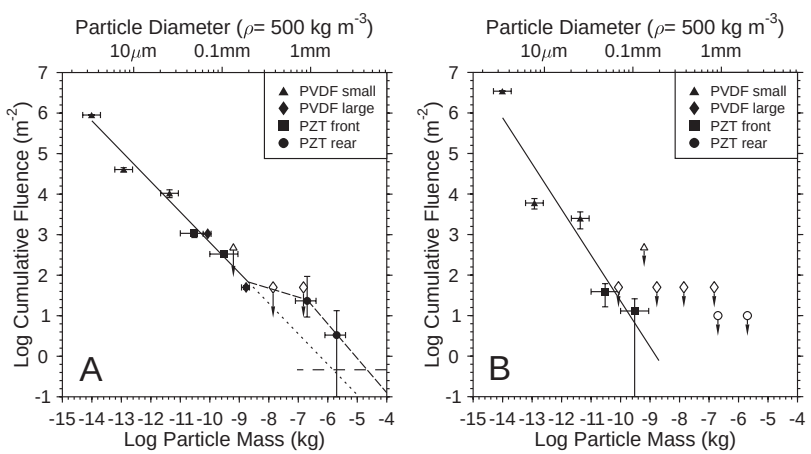

Fig. 4. (**A**) The cumulative mass distribution in the inner coma of Wild 2 [particles detected within 600 s of closest approach (r < 3700 km)]. Open symbols with arrows indicate upper limits corresponding to one impact. The solid line is the best fit mass distribution (α = 0.75) for m < 10^{-9} kg. At larger masses an excess of larger particles (dashed line), similar to that seen in Halley, fits the limited data available better than an extrapolation of the distribution at small sizes (dotted line). (**B**) Cumulative mass distribution for particles detected after +600 s, where the best fit mass distribution (α = 1.13) indicates a dominance of small particles.

spacecraft. Both types of event are seen in Fig. 2.

Although the location of the second high-activity period and its narrow size distribution are consistent with the terminator shock for micrometer-sized grains predicted by (*16*), the structure within it and the sheer intensity of the bursts are not predicted and may also provide evidence for fragmentation. An alternative explanation is activity from, or fragmentation of, a large (meter-sized) particle ejected at low velocity at a previous apparition (*17*).

Of the previous cometary flybys, there are no comparable dust detection experiment data. There was no evidence of the type of structure seen by DFMI in the Giotto Dust Impact Detection System data at 1P/Halley (*18*). However, the higher encounter speed and lower time resolution gave a spatial resolution 120 times lower than that of Stardust. At this resolution, the small-scale structure seen in the 1P/Halley data (*19*) is consistent with that seen at Wild 2. The Vega 1 and 2 dust experiments (*7*–*9*) sampled the coma beyond 8000 km, where the angular sizes of structures would be much larger. The role of fragmentation in cometary comae is discussed further by Clark *et al*. (*20*).

The cumulative fluence in the coma up to +600 s (i.e., excluding the major postencounter swarms of particles) has been calculated for each sensor subsystem (Fig. 4A). The PVDF small and large sensors and the front shield acoustic sensors represent independent data sets but are consistent, with a single-slope cumulative mass distribution of $\alpha = 0.75 \pm 0.05$. The coma scattered light is dominated by small particles, whereas the total mass in the coma is dominated by the large particles. Despite very large variations in the mass distribution on small scales (as evidenced by Fig. 2), this average mass distribution is similar to that found at 1P/Halley (*18*) and is entirely consistent with the total dust content of the coma predicted from ground-based data (*21*). The average mass distribution may contain some structure and in particular may show a large particle excess similar to that seen at 1P/Halley at masses above 10^{-9} kg (*18*, *22*). This may be confirmed when individual particle masses are determined for the detections with the acoustic sensors. The mass distribution for the period after +600 s is shown in Fig. 4B. No shield penetrations were detected, consistent with the very high cumulative mass index $\alpha = 1.13 \pm 0.2$.

The mass distributions in Fig. 4 can be used to estimate the number of particles in the aerogel collectors and also the largest particle impacting the spacecraft. The primary objective of Stardust was to collect at least 1000 particles with diameters of 15 μm or larger.

The densities of cometary grains are highly uncertain and probably mass-dependent, with large, low-density particles formed of open structures of higher density submicrometer silicate, organic, or volatile components. For the larger grains, densities as low as 50 kg m^{-3} may be possible, with 500 kg m^{-3} a likely upper limit (*23*). Here, we assume a density of 500 kg m^{-3} (such that a 15-μm particle has a mass of 8.8×10^{-13} kg), which gives a conservative estimate of the number of 15-μm particles captured (a lower density would indicate a larger number of captured particles at this size). A collector area of 0.1039 m^2 (*24*) implies 2300 ± 400 particles collected in the inner coma and 500 ± 200 from the postencounter swarm. The estimated largest single mass impacting the aerogel is $\sim 6 \times 10^{-7}$ kg (≈1.3 mm in diameter), which dominates the total collected mass.

References and Notes

1. A. J. Tuzzolino *et al*., *J. Geophys. Res.* **108**, 10.1029/2003JE002086 (2003).
2. In each test of the onset of noisy operation, the power consumption increased drastically and the spacecraft flight software generated multiple error event reports (EVRs). A software patch was implemented to turn the DFMI off if it went into a noisy state. The noise started in all counters at the same time, and in the most sensitive case (m1 counter) it saturated the counter in a few seconds. Nothing similar was observed during the Wild 2 encounter: We have not seen any noise, no EVRs were generated, and the instrument was not turned off by the software patch. In addition, the calibration performed immediately after the encounter showed nominal expected performance, and the instrument was turned off before it went noisy, some 2000 s after it was turned on.
3. More information is available at http://stardust.jpl.nasa.gov/news/news94.html.
4. J. A. Simpson *et al*., *Nature* **321**, 278 (1986).
5. J. A. Simpson *et al*., in *Symposium on Diversity and Similarity of Comets*, Brussels, Belgium, 6 to 9 April 1987 (European Space Agency Special Publication No. 278, Paris, 1987), p. 391.
6. J. A. Simpson *et al*., *Adv. Space Res.* **9**, 259 (1989).
7. E. P. Mazets *et al*., *Astron. Astrophys.* **187**, 699 (1987).
8. O. L. Vaisberg *et al*., *Astron. Astrophys.* **187**, 753 (1987).
9. J. A. Simpson, D. Rabinowitz, A. J. Tuzzolino, L. V. Ksanfomality, R. Z. Sagdeev, *Astron. Astrophys.* **187**, 742 (1987).
10. A. V. Rodoniov, J.-F. Crifo, K. Szegö, J. Lagerros, M. Fulle, *Planet. Space Sci.* **50**, 983 (2002).
11. J.-F. Crifo, A. V. Rodionov, K. Szegö, M. Fulle, *Earth Moon Planets* **90**, 227 (2002).
12. More information is available at http://stardust.jpl.nasa.gov/photo/cool.html.
13. R. L. Newburn, T. C. Duxbury, D. E. Brownlee, in preparation.
14. N. Thomas, H. U. Keller, *Astron. Astrophys.* **187**, 843 (1987).
15. L. A. Soderblom *et al*., *Icarus* **167**, 4 (2004).
16. J. F. Crifo, A. V. Rodionov, D. Bockelée-Morvan, *Icarus* **138**, 85 (1999).
17. Z. Sekanina *et al*., *Science* **304**, 1769 (2004).
18. J. A. M. McDonnell *et al*., *Astron. Astrophys.* **187**, 719 (1987).
19. A. C. Levasseur-Regourd, N. McBride, E. Hadamcik, M. Fulle, *Astron. Astrophys.* **348**, 636 (1999).
20. B. C. Clark *et al*., in preparation.
21. M. Hanner, personal communication.
22. J. A. M. McDonnell, P. L. Lamy, G. S. Pankiewicz, in *Comets in the Post-Halley Era*, R. L. Newburn, M. Neugebauer, J. Rahe, Eds. (Kluwer, Dordrecht, Netherlands, 1991), vol. 2, pp. 1043–1073.
23. M. Fulle, A. C. Levasseur-Regourd, N. McBride, E. Hadamcik, *Astron. J.* **119**, 1968, (2000).
24. P. Tsou, D. E. Brownlee, S. A. Sandford, F. Horz, M. E. Zolensky, *J. Geophys. Res.* **108**, 10.1029/2003JE002109 (2003).
25. We thank F. Di Donna and P. Di Donna for their important contributions to the design, construction, testing, and calibration of the DFMI; E. Larue for construction of the DFMI PVDF sensors; and B. McKibben for support during the initial stage of the Stardust program. The University of Chicago effort was supported by Lockhead Martin Astronautics contract RF6-457089. The group at the Open University acknowledges receipt of a grant from Particle Physics and Astronomy Research Council (United Kingdom).

5 April 2004; accepted 28 May 2004